Global drought and severe drought affected population in 1.5°C and 2°C warmer worlds

Wenbin Liu[a], Fubao Sun[a,b,c,d*], Wee Ho Lim[a,e], Jie Zhang[a], Hong Wang[a], Hideo Shiogama[f] and Yuqing Zhang[g]

[a] Key Laboratory of Water Cycle and Related Land Surface Processes, Institute of Geographic Sciences and Natural Resources Research, Chinese Academy of Sciences, Beijing, China

[b] Ecology Institute of Qilian Mountain, Hexi University, Zhangye, China

[c] College of Resources and Environment, University of Chinese Academy of Sciences, Beijing, China

[d] Center for Water Resources Research, Chinese Academy of Sciences, Beijing, China

[e] Environmental Change Institute, University of Oxford, Oxford, UK

[f] Center for Global Environmental Research, National Institute for Environmental Studies, Tsukuba, Japan

[g] College of Atmospheric Sciences, Nanjing University of Information Science and Technology, Nanjing, China

Pre-submit to: Earth System Dynamics (*Special issue: Earth System at a 1.5°C warming world*)

Corresponding to: Prof. Fubao Sun (*sunfb@igsnrr.ac.cn*), Institute of Geographic Sciences and Natural Resources Research, Chinese Academy of Sciences

2018/1/19

Abstract. The 2015 Paris Agreement proposed a more ambitious climate change mitigation target, on limiting the global warming at 1.5^{o}C instead of 2^{o}C above pre-industrial levels. Scientific investigations on environmental risks associated with these warming targets are necessary to inform climate policymaking. Based on the CMIP5 (the fifth Coupled Model Intercomparison Project) climate models, we present the first risk-based assessment of changes in global drought and the impact of severe drought on population at 1.5^{o}C and 2^{o}C additional warming conditions. Our results highlight the risk of drought at the globe (drought duration would increase from 2.9 to 3.1~3.2 months) and in several hotspot regions such as Amazon, Northeastern Brazil, South Africa and Central Europe at both 1.5 ^{o}C and 2 ^{o}C global warming relative to the historical period. Correspondingly, more total and urban population would be exposed to severe droughts at the globe (+132.5±216.2 million and +194.5±276.5 million total population, +350.2±158.8 million and +410.7±213.5 million urban population in 1.5 ^{o}C and 2 ^{o}C warmer worlds) and some regions (i.e., East Africa, West Africa and South Asia). Less rural population would be exposed to severe drought at the globe under both climate warming and population growth (especially the urbanization-induced population migration). By keeping global warming at 1.5^{o}C above the pre-industrial levels instead of 2^{o}C, drought risks would decrease (i.e., less drought duration, drought intensity and drought severity but relatively more frequent severe drought) and the affected total, urban and rural population would decrease at the globe and in most regions. Whilst challenging for both East Africa and South Asia, the benefits of limiting warming to below 1.5^{o}C in terms of global drought risk and impact reduction are significant.

1 Introduction

Drought could bring adverse consequences on water supplies, food productions and the environment (Wang et al., 2011; Sheffield et al., 2012). Because of these serious consequences, severe droughts in the recent past have gained wide attentions, these include the Millennium drought in Southeast Australia (van Dijk et al., 2013; Kiem et al., 2016), the once-in-a-century droughts in Southwest China (Qiu, 2010, Zuo et al., 2015), the Horn of Africa drought (Masih et al., 2014; Lyon, 2014) and the most recent California drought (Aghakouchak et al., 2015; Cheng et al., 2016). In the context of climate change, drought risks (i.e., drought duration and intensity) are likely to increase in many historical drought-prone regions with global warming (Dai et al., 2012; Fu and Feng, 2014; Kelley et al., 2015; Ault et al., 2016). A better understanding of changes in global drought characteristics and their socioeconomic impacts in the 21st century should feed into long-term climate adaptation and mitigation plans.

The United Nations Framework Convention on Climate Change (UNFCCC) agreed to establish a long-term temperature goal for climate projection of "*pursue efforts to limit the temperature increase to 1.5^{o}C above pre-industrial levels, recognizing that this would significantly reduce the risks and impacts of climate change*" (UNFCCC Conference of the Parties, 2015) in the 2015 Paris Agreement, and invited the Intergovernmental Panel on Climate Change (IPCC) to announce a special report "*On the impacts of global warming of 1.5^{o}C above pre-industrial levels and related greenhouse gas emission pathways*" in 2018 (Mitchell et al., 2016). Regardless of the socio-economic and political achievability of this goals (Sanderson et al., 2017), there is a paucity of scientific knowledge about the relative risks (i.e., drought risks and their potential impacts) associated with the implications of 1.5^{o}C and/or 2^{o}C warming, this naturally attracted contributions from scientific community (Hulme 2016, Schleussner et al., 2016, Peters 2016, King et al., 2017).

To target on the impact assessments of 1.5^{o}C and/or 2^{o}C warming, there are currently several approaches (James et al., 2017). One way is to enable impact assessments at near-equilibrium climate of 1.5^{o}C and/or 2^{o}C warmer worlds designed specifically using a set of ensemble simulations produced by a coupled climate model (i.e., Community Earth System Model, CESM) (Sanderson et al., 2017; Wang et al., 2017). Although similar results of drought response to warming were obtained as that conducted by Coupled Model Intercomparison Project-style experiments (i.e., CMIP5, Taylor et al., 2012), the structural uncertainty and robustness of change in droughts among different climate models cannot be fully evaluated in this kind of single-model study (Lehner et al., 2017). A second approach extends the former idea to multiple climate models. For instance, the HAPPI (Half a degree Additional warming, Projections, Prognosis and Impacts) model intercomparison project provided a new assessment framework and a dataset with experiment design target explicitly to 1.5^{o}C and 2^{o}C above the pre-industrial levels (Mitchell et al., 2017). However, the analysis/calculation of drought characteristics needs data with long-term period (typically >20 consecutive years, McKee et al., 1993), the ten-year period HAPPI dataset (i.e., 2005-2016 for the historical period and 2105-2116 for the 1.5^{o}C and 2^{o}C warmer worlds) is relatively short (consecutive samples are too short for calculating a drought index, i.e., Palmer drought severity index (PDSI), Palmer, 1965) for an index-based drought assessment. A third approach utilizes the outputs of CMIP5 climate models under the RCP2.6 scenarios for this kind of "risk assessment-style" studies, but only a handful of General Circulation Models

(GCMs) simulations end up showing 1.5^{o}C global warming by end of the 21st century. Alternatively, transient simulations from multiple CMIP5 GCMs at higher greenhouse emissions (i.e., the RCP4.5 and RCP8.5) (Schleussner et al., 2016; King et al., 2017) could be analyzed in order to evaluate the potential risks of drought under different warming targets, albeit the long-duration drought years might be underestimated due to insufficient sampling of extended drought events (Lehner et al., 2017).

Here, we quantify the changes in global and sub-continental drought characteristics (i.e., drought duration, intensity and severity) at 1.5^{o}C and 2^{o}C above the pre-industrial levels and find out whether there are significant differences between them. We perform this analysis using a drought index-PDSI forced by the latest CMIP5 GCMs. To evaluate the societal impacts, we incorporate the Shared Socioeconomic Pathway 1 (SSP1) spatial explicit global population scenario and examine the exposure of population (including rural, urban and total population) to severe droughts. This paper is organized as follows: Section 2 introduces the CMIP5 GCMs output and SSP1 population data applied in this study. We define the baseline, 1.5^{o}C and 2^{o}C warmer world; and describe the calculation of PDSI-based drought characteristics and population exposure under severe droughts in this section. Section 3 shows the results (i.e., hotspots and risks) of changes in drought characteristics and the impacts of severe drought on people under these warming targets. We perform detailed discussions in Section 4 and conclude our findings in Section 5.

2 Material and Methods

2.1 Data

In this study, we use the CMIP5 GCMs output (including the monthly outputs of surface mean air temperature, surface minimum air temperature, surface maximum air temperature, air pressure, precipitation, relatively humidity, surface downwelling longwave flux, surface downwelling shortwave flux, surface upwelling longwave flux and surface upwelling shortwave flux as well as the daily outputs of surface zonal velocity component ($uwnd$) and meridional velocity component ($vwnd$)) archived at the Earth System Grid Federation (ESGF) Node at the German Climate Computing Center-DKRZ (https://esgf-data.dkrz.de/projects/esgf-dkrz/) over the period 1850-2100. In the CMIP5 archive, the monthly $uwnd$ and $vwnd$ were computed as the means of their daily values with the plus-minus sign, the calculated wind speed from the monthly $uwnd$ and $vwnd$ would be equal to or, in most cases, less than that computed from the daily values (Liu and Sun, 2016). To get the monthly wind speed, we average the daily values ($\sqrt{uwnd^2 + vwnd^2}$) over a month.

Recent studies have confirmed that the impacts of similar global mean surface temperature (i.e., 1.5^{o}C and 2^{o}C warmer worlds) among the Representative Concentration Pathways (RCPs) are quite similar, implying that the global and regional responses to temperature and are independent of the RCPs (Hu et al., 2017; King et al., 2017). Following this idea, we settled at using 11 CMIP5 models which satisfied the data requirement of PDSI calculation (see paragraph above) under RCP4.5 and RCP8.5. Following Wang et al. (2017) and King et al. (2017), we use the ensemble mean of these CMIP5 models and climate scenarios (RCP4.5, RCP8.5) to composite the warming scenarios (1.5^{o}C and 2^{o}C warmer worlds).

<Table 1, here, thanks>

To consider the people affected by severe drought events, we use the spatial explicit global population scenarios developed by researchers from the Integrated Assessment Modeling (IAM) group of National Center for Atmospheric Research (NCAR) and the City University of New York Institute for Demographic Research (Jones and O'Neil, 2016). They included the gridded population data for the baseline year (2000) and for the period of 2010-2100 in ten-year steps at a spatial resolution of 0.125 degree, which are consistent with the new Shared Socioeconomic Pathways (SSPs). We apply the population data of the SSP1 scenario, which describes a future pathway with sustainable development and low challenges for adaptation and mitigation. We upscale this product to a spatial resolution of $0.5^{o} \times 0.5^{o}$. For the global and sub-continental scales analysis, we use the global land mass between 66^{o}N and 66^{o}S (Fischer et al., 2013; Schleussner et al., 2016) and 26 sub-continental regions (as used in IPCC, 2012, see Table 2 for details).

<Table 2, here, thanks>

2.2 Definition of a baseline, 1.5^{o}C and 2^{o}C warmer worlds

To define a baseline, 1.5^{o}C and 2^{o}C warmer worlds, we first calculate the global mean surface air temperature (GMT) for each climate model and emission scenario over the period 1850-2100. We weigh the surface air temperature field by the square root of cosine (latitude) to consider the dependence of grid density on latitude (Liu et al., 2016). We compute and smooth the multi-model Ensemble Mean (MEM) GMT using a 20-year moving average filter for the RCP4.5 and RCP8.5, respectively. This study applied continuous time series for identification of drought duration, intensity and severity. From the climate model projections, we noticed that inter-annual variation of global mean air temperature is common and its magnitude differs with different climate models. To account for it, following Wang et al. (2017), we first select a baseline period of 1986-2005 for which the observed GMT was about 0.6^{o}C warmer (the MEM GMT was 0.4~0.8 ^{o}C warmer during this period in 11 climate models used) than the pre-industrial levels (1850-1900, IPCC, 2013). This is also a common reference period for climate impact assessment (e.g., Schleussner et al., 2016). Next, for each emission scenario (RCP4.5 or RCP8.5), we define the periods (Figure 1) during which the 20-year smoothed GMT increase by 1.3~1.7 ^{o}C (2027-2038 under the RCP4.5 and 2029-2047 under the RCP 8.5) and by 1.8~2.2 ^{o}C (2053-2081 under the RCP4.5 and 2042-2053 under the RCP 8.5) above the pre-industrial period as the 1.5^{o}C and 2^{o}C warmer worlds, respectively (as in King et al., 2017). To reduce the projection uncertainty inherited from different emission scenarios, we combine (by averaging) the results of drought characteristics and population exposures calculated for selected periods under the RCP4.5 and RCP8.5, to represent the ensemble means of drought risk at 1.5^{o}C or 2^{o}C warmer worlds. In the 1.5^{o}C and 2^{o}C warmer worlds, we get 372 and 492 monthly data-points, respectively.

<Figure 1, here, thanks>

2.3 Characterize global drought using PDSI

To quantify the changes in drought characteristics, we adopt the Palmer Drought Severity index (PDSI), which describes the balance between water supply (precipitation) and atmospheric evaporative demand (required “precipitation” estimated under climatically appropriate for existing conditions, CAFEC) at the monthly scale (Wells et al., 2004; Zhang et al., 2016). For a multiyear time series, this index is commonly applied as an indication of a meteorological drought; to a lesser extent, a hydrological drought (Heim Jr., 2002; Zargar et al., 2011; Hao et al., 2018). It incorporates antecedent precipitation, potential evaporation and the local Available

Water Content (AWC, links: https://daac.ornl.gov/cgi-bin/dsviewer.pl?ds_id=548) of the soil in the hydrological accounting system. It measures the cumulative departure relative to the local mean conditions in atmospheric moisture supply and demand on land surface. In the PDSI model, five surface water fluxes, namely, precipitation (*P*), recharge to soil (*R*), actual evapotranspiration (*E*), runoff (*RO*) and water loss to the soil layers (*L*); and their potential values $\hat{P}$, *PR*, *PE*, *PRO* and *PL* are considered. All values in the model can be computed under CAFEC values using the precipitation, potential evaporation and AWC inputs. For example, the CAFEC precipitation ($\hat{P}$) is defined as (Dai et al., 2011),

$$\hat{P} = \frac{\overline{E_i}}{\overline{PE_i}} PE + \frac{\overline{R_i}}{\overline{PR_i}} PR + \frac{\overline{RO_i}}{\overline{PRO_i}} PRO - \frac{\overline{L_i}}{\overline{PL_i}} PL, \quad (1)$$

In Equation 1, the over bar indicates averaging of a parameter over the calibration period. The moisture anomaly index (*Z* index) is derived as the product of the monthly moisture departure ($P - \hat{P}$) and a climate characteristics coefficient *K*. The *Z* index is then applied to calculate the PDSI value for time $t(X_t)$:

$$X_t = pX_{t-1} + qZ_t = 0.897X_{t-1} + Z_t/3 \quad (2)$$

Where X_{t-1} is the PDSI of the previous month, and p and q are duration factors. The calculated PDSI ranges -10 (dry) to 10 (wet). The parameters (i.e., the duration factor) in PDSI model are calibrated using the period 1850-2000 (see Section 2.2).

As part of the PDSI calculation, we quantify the potential evaporation (PET) using the Food and Agricultural Organization (FAO) Penman-Monteith equation (Allen et al., 1998),

$$PET = \frac{0.408\Delta(R_n - G) + \gamma\frac{900}{T+273}U_2 e_s(1 - \frac{Rh}{100})}{\Delta + \gamma(1 + 0.34U_2)} \quad (3)$$

where Δ is the slope of the vapor pressure curve, U_2 is the wind speed at 2 m height, G is the soil heat flux, Rh is the relative humidity, γ is the psychometric constant, e_s is the saturation vapor pressure at a given air temperature (T). R_n is the net radiation which can be calculated using the surface downwelling/upwelling shortwave and longwave radiations. We estimate all other parameters in the FAO Penman-Monteith equation using the GCM outputs through the standard algorithm as per recommended by the FAO (Allen et al., 1998). In this study, we perform this calculation for each GCM over the period 1850-2100 using the tool for calculating the PDSI (the original MATLAB codes were modified for this case) developed by Jacobi et al. (2013).

Based on the calculated global PDSI, we derive the drought characteristics (i.e., drought duration, drought intensity and drought severity) using the run theory for the baseline, 1.5°C and 2°C warmer worlds, respectively. Briefly, the concept of “run theory” is proposed by Yevjevich and Ingenieur (1967). The run characterizes the statistical properties of sequences in both time and space. It is useful for defining drought in an objective manner. In the run theory, a “run” represents a portion of time series $\mathrm{X_i}$, where all values are either below or above a specified threshold (we set the threshold PDSI < -1 in this study) (Ayantobo et al., 2017). We define a “run” with values continuously stay below that threshold (i.e., negative run) as a drought event, which generally includes these characteristics: drought duration, drought intensity and drought severity (see Figure 2 for better illustration). We define the drought duration (months in this study) as a period (years/months/weeks) which PDSI stays below a specific threshold (PDSI < -1). Drought severity (dimensionless) indicates a cumulative deficiency of a drought event below the threshold (PDSI < -1), while drought intensity (dimensionless) is the average value of a drought event below this threshold (Mishra and Singh, 2010). For each GCM, we calculate the medians of drought duration, drought intensity and drought severity at each grid-cell across all drought events for each selected period (i.e., the baseline, 1.5^{o}C and 2^{o}C warmer worlds). It should be noted that the global PDSI and related drought characteristics were first calculated using GCM-outputs with their original spatial resolution. The obtained results were then rescaled to a common spatial resolution of 0.5^{o} ×0.5^{o} using the bilinear interpolation, in order to show them with a finer resolution uniformly and accommodate their spatial resolution to that of SSP1 population (0.5^{o} ×0.5^{o}). The original resolution of SSP1 population is 0.125 degree. We thus use a 0.5 degree resolution to avoid effectively making up data of the finer resolution in SSP1 data. We synthesize the results by evaluating the ensemble mean and model consistency/inter-model variance across all climate models.

<Figure 2, here, thanks>

2.4 Calculation of population exposure under severe droughts

Following Wells et al. (2014), when monthly PDSI < -3, we assume a severe drought event took place. If a severe drought occurred for at least a month in a year, we would take that year as a severe drought year. For each GCM per period (i.e., the baseline, 1.5^{o}C and 2^{o}C warmer worlds), we quantify the population (including urban, rural and all population) affected by severe drought per grid-cell as (population × annual frequency of severe drought). We first compute the affected population for the baseline period (1985-2005) using the SSP1 base year (2000). We repeat this estimation using the constant SSP1 population data in 2100 for the 1.5^{o}C and 2^{o}C warming worlds, which is consistent with the original proposal of Paris Agreement on stabilizing global warming for the specified targets by end of the 21st century. We used SSP1 scenario because it describes the storyline of a green growth paradigm with sustainable development and low challenges for adaptation and mitigation (Jones and O'Niell, 2016). The 1.5^{o}C and 2^{o}C warmer worlds clearly fit in this description and thus considered under the 2015 Paris Agreement (UNFCCC Conference of the Parties 2015; O'Niell et al., 2016). In this pathway, the world population would peak at around 2050s and then decline (van Vuuren et al., 2017). The environmental friendly living arrangements and human settlement design in this scenario would lead to fast urbanization in all countries. More in-migrants from rural areas would be attracted to cities due to more adequate infrastructure, employment opportunities and convenient services for their residents (Cuaresma, 2012). The world urban population would gradually increase while rural population would correspondingly decline in the future under SSP1 scenario.

3 Results

3.1 Changes in PDSI and drought characteristics

We present the changes in multi-model ensemble mean PDSI from the baseline period (1986-2005) to each of the 1.5^{o}C and 2^{o}C scenarios and model consistency in Figure 3. For the 1.5^{o}C warmer world, the PDSI would decrease (more drought-prone) with relatively higher model consistency (6~11 models in totally 11 climate models) in some regions, for example, Amazon (0.7±0.8 -> -0.1±0.2), Northeastern Brazil (0.5±0.6 -> -0.1±0.3), Southern Europe and Mediterranean (0.4±0.6 -> -0.3±0.2), Central America and Mexico (0.2±0.4 -> -0.2±0.1), Central Europe (0.3±1.0 -> -0.1±0.4) as well as Southern Africa (0.5±0.5 -> -0.3±0.2); slightly increase (less drought-prone) in Alaska/Northwest Canada (-0.01±0.5 -> -0.3±0.2) and North Asia (-0.1±1.0 -> -0.2±0.2) but with relatively low model consistency. The geographic pattern of changes in PDSI for the 2^{o}C warmer world is quite similar to that of 1.5^{o}C warmer world, but the magnitude of change would intensify (in both direction) East Canada, Greenland, Iceland (-0.3±0.2-> -0.4±0.2), East Africa (-0.5±0.2-> -0.3±0.2), Northern Europe (-0.3±0.3-> -0.2±0.3), East Asia (-0.3±0.1-> -0.2±0.4), South Asia (-1.0±1.2-> -0.8±0.3) and West Africa (-0.3±0.2-> -0.3±0.3). When global warming is capped at 1.5^{o}C instead of 2^{o}C above the pre-industrial levels, the PDSI value would elevate at the globe (66^{o}S-66^{o}S, -0.4±0.2-> -0.3±0.2) and most regions (Alaska/Northwest Canada, East Africa, West Africa, Tibetan Plateau, North Asia, East Asia, South Asia and Southeast Asia) (Figure 4).

<Figure 3, here, thanks>

<Figure 4, here, thanks>

We analyze the changes in drought characteristics such as its duration, severity and intensity in 1.5^{o}C and 2^{o}C warmer worlds. In terms of the drought duration (Figures 5-6), we find robust large-scale features. For example, the drought duration would generally increase at the globe (2.9±0.5 -> 3.1±0.4 months and 2.9±0.5 -> 3.2±0.5 months from the baseline period to the 1.5^{o}C and 2^{o}C scenarios) and most regions (especially for Amazon, Sahara, Northeastern Brazil and North Australia) except for North Asia (2.7±0.6 -> 2.6±0.5 months and 2.7±0.6 -> 2.5±0.4 months) in both worlds. The high model consistency in most regions (i.e., Amazon, Sahara and Northeastern Brazil) for both warming targets gives us more confidence on these projections. Relative to the 2^{o}C warmer target, a 1.5^{o}C warming target is more likely to reduce drought duration at both global and regional scales (except for Alaska/Northwest Canada, East Africa, Sahara, North Europe, North Asia, South Asia, Southeast Asia, Tibetan Plateau and West Africa).

<Figure 5, here, thanks>

<Figure 6, here, thanks>

Drought intensity and drought severity are commonly used for quantifying the extent of water availability drops significantly below normal conditions in a region. In this study, the drought intensity is projected to increase at the globe (0.9±0.3 -> 1.1±0.3 and 0.9±0.3 -> 1.0±0.2 from the baseline period to the 1.5^{o}C and 2^{o}C scenarios) and in most of the regions except for North Asia, Southeast Asia and West Africa in 1.5^{o}C and 2^{o}C warmer worlds (Figures 7-8). Compare to the 2^{o}C warmer world, the drought intensity would obviously relieve at the global and sub- continental scales except for East Canada, Greenland, Iceland (1.0±0.6 -> 0.8±0.5) and West North America (0.9±0.3 -> 0.8±0.2) in the 1.5^{o}C warmer world. In addition, the projected drought severity would also increase in these warmer worlds at the globe (3.0±1.9 -> 4.5±3.0 and 3.0±1.9 -> 3.8±2.0 from the baseline period to the 1.5^{o}C and 2^{o}C warmer worlds) and in most regions except for North Asia (1.8±0.6 -> 1.8±0.7 and 1.8±0.6 -> 1.5±0.3) (Figures 9-10). When global warming is maintained at 1.5^{o}C instead of 2^{o}C above the pre-industrial levels, the drought severity would weaken in most regions except for Sahara (3.1±0.9-> 3.5±1.3), North Asia (1.5±0.3 -> 1.8±0.8), Southeast Asia (17.2±20.1 -> 35.8±57.2), and West North America (2.4±1.7 -> 2.5±1.4). The projected uncertainties are relatively low (6~11 models in totally 11 models) for the changes of each drought characteristic in these warming scenarios all over the world, except for some parts of Alaska/Northwest Canada, East Canada, Greenland, Iceland, West North America, Central North America, East North America, Sahara, West Africa, East Africa and North Asia.

<Figure 7, here, thanks>

<Figure 8, here, thanks>

3.2 Impact of severe drought on population

To understand the societal influences of severe drought, we combine the drought projection with SSP1 population information and estimate the total, urban and rural population affected by severe drought in the baseline period, $1.5^{o}C$ and $2^{o}C$ warmer worlds (Figures 11-13). Compare to the baseline period, the frequency of severe drought (PDSI < -3), drought-affected total and urban population would increase in most of the regions in $1.5^{o}C$ and $2^{o}C$ warmer worlds. Globally, we estimate that 132.5±216.2 million (350.2±158.8 million urban population and -217.7±79.2 million rural population) and 194.5±276.5 million (410.7±213.5 million urban population and -216.2±82.4 million rural population) additional people would be exposed solely to severe droughts in the $1.5^{o}C$ and $2^{o}C$ warmer worlds, respectively. The severe drought affected total population would increase under these warming targets in most regions, except for East Asia, North Asia, South Asia, Southeast Asia, Tibetan Plateau and West Coast South America.

<Figure 9, here, thanks>

<Figure 10, here, thanks>

The severe drought affect urban (rural) population would increase (decrease) in all global regions in $1.5^{o}C$ and $2^{o}C$ warmer worlds. For example, the projections suggest that more urban population would be exposed to severe drought in Central Europe (10.9±7.7 million), Southern Europe and Mediterranean (14.0±4.6 million), West Africa (65.3±34.1 million), East Asia (16.1±16.0 million), West Asia (16.2±7.4 million) and Southeast Asia (24.4±19.7 million) in $1.5^{o}C$ warmer world relative to the baseline period. We also find that the number of affected people would escalate further in these regions in $2^{o}C$ warmer world. In terms of the rural population, less people in Central Asia (-4.1±4.7 million and -3.3±4.1 million for the $1.5^{o}C$ and $2^{o}C$ warmer worlds), Central North America (-0.5±1.1 million and -0.4±0.9 million), Southern Europe and

Mediterranean (-3.6±3.2 million and -2.9±3.8 million), South Africa (-3.3±1.5 million and -2.9±1.8 million), Sahara (-1.0±2.5 million and -0.9±2.9 million), South Asia (-70.2±29.7 million and -72.9±30.0 million), Tibetan Plateau (-2.3±1.8million and -2.1±1.9 million) and West North America (-1.7±1.0 million and -1.6±1.1 million) would be exposed to the severe drought in 1.5^{o}C and 2^{o}C warmer worlds relative to the baseline period. The distinct influences of severe drought on urban and rural population are driven by both climate warming and population growth, especially by the urbanization-induced population migration.

<Figure 11, here, thanks>

<Figure 12, here, thanks>

When global warming approaches 1.5^{o}C (instead of 2^{o}C) above the pre-industrial levels, relatively less total, urban and rural population (except for East Africa and South Asia) would be affected despite more frequent severe drought in most regions such as East Asia, Southern Europe and Mediterranean, Central Europe and Amazon. This implies that the benefit of holding global warming at 1.5^{o}C instead of 2^{o}C is apparent to the severe-drought affected total, urban and rural population in most regions, but challenges remain in the East Africa and South Asia.

<Figure 13, here, thanks>

4 Discussions

The changes in PDSI, drought duration, intensity and severity with climate warming (i.e., 1.5^{o}C and 2^{o}C warmer worlds) projected in this study is in general agreement with that concluded by IPCC (2013) despite regional variation. For example, as revealed in this study, the gradual decline of PDSI (drought-prone) in American Southwest and Central Plains was also projected using an empirical drought reconstruction and soil moisture metrics from 17 state–of-the-art GCMs in the

21st century (Cook et al., 2015). The ascending risk of drought in Sahara, North Australia and South Africa coincided with Huang et al. (2017), which projected that global drylands would degrade in 2°C warmer world. Moreover, the increases in drought duration, intensity and severity in Central America, Amazon, South Africa and Mediterranean are in agreement with the extension of dry spell length and less water availability in these regions under the 1.5°C and/or 2°C warming scenarios (Schleussner et al., 2016; Lehner et al., 2017). In addition, we find that the affected population attributes more (50%~75%) to the population growth rather than the climate change driven severe drought in the 1.5°C and 2°C warmer worlds. This number is greater than that concluded by Smirnov et al. (2016), maybe due to different study periods, population data, drought index and warming scenarios used.

Projections presented in current study inherited several sources of uncertainty. Firstly, there are considerable uncertainties in the numerical projections from different climate models under varied greenhouse gas emission scenarios, especially on a regional scale (i.e., Sahara, Alaska/Northwest Canada and North Asia). However, the utility of multiple GCMs and emission scenarios should allow us to synthesize future projections better than single model/scenario analysis (Schleussner et al., 2016; Wang et al., 2017; Lehner et al., 2017). On top of that, we performed uncertainty analysis such as understanding the model consistency (e.g., increase/decrease) and inter-model variance (for magnitude changes). These enable us to characterize regional and global projections which could vary due to different model structure of GCMs and how they behave under different RCP scenarios. Moreover, the global and regional responses (i.e., warming/precipitation patterns) to varied warming scenarios (i.e., 1.5°C and 2°C) showed little dependences on RCP scenarios (King et al., 2017; Hu et al., 2017). Therefore, the uncertainty caused by the choice of RCP scenarios might be small. Secondly, there are various ways of picking the 1.5^{o}C or 2^{o}C warming signals (King et al., 2017). Current study considered both the influences of multi-model and multi-scenario for each warming scenario using the 20-year smoothed multi-model ensemble mean GMT. The selected periods of 1.5^{o}C and 2.0^{o}C warmer worlds are close to that of King et al. (2017). Finally, the SSP1 population data and the single drought index used might introduce uncertainties. Despite these sources of uncertainty, these projections are quite robust with high model consistency across most regions.

This analysis evaluated the risk of droughts in terms of how they would change in the future period (1.5^{o}C or 2^{o}C warmer worlds) relative to the baseline period; and the difference between the two warmer worlds. In this perspective, uncertainty arises from climate model bias in between two periods more or less cancels each other. Previous studies demonstrated that bias-corrections do not yield much difference in such circumstance (e.g., Sun et al., 2011; Maraun, 2016). In addition, the methodology here requires the meteorological information with physical meaning (see Section 2.1) that is consistent with the energy balance of the climate model (Equation 3 in Section 2.3), hence existing bias-correction measures (with known weakness in maintaining the physical aspect of bias-corrected output) appears less feasible. (Future innovation which accounts for both statistics and energy balance of climate model output in new bias-correction methodology for handling the high non-linear outcomes should be a subject of scientific interest.) The rationale of using model consistency (Figures 3, 5, 7, 9) as a form of "confidence index" here emerges from the idea that, whilst model validation in historical period is helpful, it does not necessary reveal the ability of each climate model in projection of risk change. Thus this kind of confidence index is informative for synthesizing multi-model projections, probably explains why it is still common in many global studies involving multi-model ensembles (e.g., Hirabayashi et al., 2013; Koirala et al., 2014).

5 Conclusions

Motivated by the 2015 Paris Agreement proposal, we analyzed the CMIP5 GCM output and presented the first comprehensive assessment of changes in drought characteristics and the potential impacts of severe drought on population (total, urban and rural) in 1.5°C and 2°C warmer worlds. We found that the risk of drought would increase (i.e., decrease in PDSI, increase in drought duration, drought intensity and drought severity) globally and most regions (i.e., Amazon, Northeastern Brazil, Central Europe) for in 1.5°C and 2°C warmer worlds relative to the baseline period (1986-2005). However, the amplitudes of change in drought characteristics vary among the regions. Relative to the 2°C warming target, a 1.5°C warming target is more likely to reduce drought risk (less drought duration, drought intensity and drought severity but relatively more frequent severe drought) significantly on both global and regional scales. The high model consistency (6~11 out of 11 GCMs) across most regions (especially Amazon, Sahara and Northeastern Brazil) gives us more confidence on these projections.

Despite the uncertainties inherited from the GCMs and population data used, as well as the definition of the 1.5°C and 2°C periods, we found significant changes of drought characteristics under both warming scenarios and societal impacts of severe drought by limiting temperature target at 1.5 ^{o}C instead of 2 ^{o}C in several hotspot regions. More total (+132.5±216.2 million and +194.5±276.5 million globally) and urban population (+350.2±158.8 million and +410.7±213.5 million globally) would be exposed to severe drought in most regions (especially East Africa, West Africa and South Asia) in 1.5 ^{o}C and 2 ^{o}C warmer worlds, particularly for the latter case.

Meanwhile, less rural population (-217.7±79.2 million and -216.2±82.4 million globally) in, e.g., Central Asia, East Canada, Greenland, Iceland, Central North America, Southern Europe and Mediterranean, North Australia, South Africa, Sahara, South Asia, Tibetan Plateau and West North America would be affected. When global mean temperature increased by 1.5 ^{o}C instead of 2 ^{o}C above the pre-industrial level, the total, urban and rural population affected by severe drought would decline in most regions except for East Africa and South Asia.

In general, this comprehensive global drought risk assessment should provide useful insights for international decision-makers to develop informed climate policy within the framework of the 2015 Paris Agreement. Whist most regions would benefit from reduced societal impacts in the 1.5 ^{o}C wamer world, local governments in East Africa and South Asia should be prepared to deal with drought-driven challenges (see paragraph above). Future studies on understanding the causes of changes in global and regional droughts (e.g., changing pattern/duration of precipitation and evaporative demand) with respect to these warming targets should assist drought risk adaptation and mitigation planning.

Data availability. The datasets applied in this study are available at the following locations:

— CMIP5 model experiments (Taylor et al., 2012), https://esgf-data.dkrz.de/projects/esgf-dkrz/

— Spatial population scenarios (Shared Socioeconomic Pathway 1, SSP1, Jones and O'Niell, 2016), https://www2.cgd.ucar.edu/sections/tss/iam/spatial-population-scenarios

Competing interests. The authors declare that they have no conflict of interest.

Acknowledgements. This study was financially supported by the National Research and Development Program of China (2016YFA0602402 and 2016YFC0401401), the National Natural Sciences Foundation of China (41401037), the Key Research Program of the Chinese Academy of Sciences (ZDRW-ZS-2017-3-1), the CAS Pioneer Hundred Talents Program (Fubao Sun) and the CAS President's International Fellowship Initiative (Wee Ho Lim, 2017PC0068). We thank the Editor (Michel Crucifix), Dimitri Defrance and an anonymous reviewer for their helpful comments.

References

Aghakouchat, A., Cheng L., Mazdiyasni, O., and Farahmand, A.: Global warming and changes in risk of concurrent climate extremes: insights from the 2014 California drought, Geophys. Res. Lett., 41, 8847-8852, doi:10.1002/2014GL062308, 2015.

Allen, R., Pereira, L.S., Raes, D., and Smith, M.: Crop evapotranspiration guidelines for computing crop water requirements-FAO Irrigation and drainage paper 56, FAO-Food and Agriculture Organization of the United Nations, Rome, 1998.

Ault, T.R., Mankin, J.S., Cook, B.I., and Smerdon, J.E.: Relative impacts of mitigation, temperature, and precipitation on 21st-century megadrought risk in the American Southwest, Sci. Adv., 2, 1-9, doi:10.1126/sciadv.1600873, 2016.

Ayantobo, O.O., Li, Y., Song, S.B., and Yao, N.: Spatial comparability of drought characteristics and related return periods in mainland China over 1961-2013, J. Hydrol., 550, 549-567, doi:10.1016/j.jhydrol.2017.05.019, 2017.

Cheng, L., Hoerling, M., Aghakouchak, A., Livneh, B., Quan, X.W., and Eischeid, J.: How has human-induced climate change affected California drought risk? J. Clim., 29, 111-120, doi:10.1175/JCLI-D-15-0260.1, 2016.

Cook, B,I., Ault, T.R., Smerdon, J.E.: Unprecedented 21^{st} century drought risk in the American Southwest and Central Plains, Sci. Adv., 1, e1400082, 2015.

Cuaresma, J.: SSP economic growth projections: IIASA model. In supplementary note for the SSP data sets. https://secure.iiasa.ac.at/web-apps/ene/SspDb/static/download/ssp_suplementary%20text.pdf, 2012.

Dai, A.G.: Characteristics and trends in various forms of the Palmer drought severity index during 1900-2008, J.Geophys.Res., 116, D12115, doi: 10.1029/2010JD015541, 2011.

Dai, A.G.: Increasing drought under global warming in observations and models, Nat. Clim. Change,3, 52-58, doi: 10.1038/NCLIMATE1633, 2012.

Fischer, E.M., Beyerle, U., and Knutti, R.: Robust spatially aggregated projections of climate extremes, Nat. Clim. Change, 2, 1033-1038, doi:10.1038/nclimate2051, 2013.

Fu, Q., and Feng, S.: Responses of terrestrial aridity to global warming, J. Geophys. Res., 119, 7863-7875, doi: 10.1002/2014JD021608, 2014.

Hao, Z.C., Singh, V.P., Xia, Y.L.: Seasonal drought prediction: advances, challenges, and future prospects. Rev. Geophys., doi: 10.1002/2016/RG000549.

Heim Jr. R.R.: A review of twentieth-century drought indices used in the United States, BAMS, 1149-1165.

Hirabayashi, Y., Mahendran, R., Korala, S., Konoshima, L., Yamazaki, D., Watanabe, S., Kim, H. and Kanae, S.: Global flood risk under climate change, Nat. Clim. Change, 3, 816-821, doi: 10.1038/nclimate1911, 2013.

Hu, T., Sun, Y., and Zhang, X.B.: Temperature and precipitation projection at 1.5 and 2oC increase in global mean temperature (in Chinese), Chin. Sci. Bull., 62, 3098-3111, doi: 10.1360/N972016-01234, 2017.

Hulme, M.: 1.5^{o}C and climate research after the Paris Agreement, Nat. Clim. Change, 6, 222-224, doi:10.1038/nclimate2939, 2016.

IPCC: Managing the Risks of Extreme Events and Disasters to Advance Climate Change Adaptation, in: A Special Report of Working Group I and II of the Intergovernmental Panel on Climate Change, edited by: Field, C.B., Barros, V., Stocker, T.F., Qin, D., Dokken, D.J., Ebi, K.L., Mastrandrea, M.D., Mach, K.J., Plattner, G.-K., Allen, S.K., Tignor, M., and Midgley, P.M., Cambridge University Press, Cambridge, UK and New York, NY, USA, 582 pp, 2012.

IPCC: Summary for Policymakers, in: Climate Change 2013: The Physical Science Basis, Contribution of Working Group I to the Fifth Assessment Report of the Intergovernmental Panel on Climate Change, edited by: Stocker, T., Qin, D., Plattner, G.-K., Tignor, M., Allen, S., Boschung, J., Nauels, A., Xia, Y., Bex, V., and Midgley, P., IPCC AR WGI, Cambridge University Press, Cambridge, UK and New York, NY, USA, 1-100, 2013.

Jacobi, J., Perrone, D., Duncan, L.L., and Hornberger, G.: A tool for calculating the Palmer drought indices, Water Resour. Res., 49, 6086-6089, doi: 10.1002/wrcr.20342, 2013.

James, R., Washington, R., Schleussner, C.-F., Rogelj, J., and Conway, D.: Characterizing half-a-degree difference: a review of methods for identifying regional climate responses to global warming target, WIREs Clim. Change, 8, e457, doi: 10.1002/wcc.457, 2017.

Jones, B. and O'Neill, B.C.: Spatially explicit global population scenarios consistent with the Shared Socioeconomic Pathways, Environ. Res. Lett., 11, 084003, http://iopscience.iop.org/1748-9326/11/8/084003, 2016.

Kelley, C.P., Mohtadi, S., Cane, M.A., Seager, R., and Kushnir, Y.: Climate change in the Fertile Crescent and implications of the recent Syrian drought, Proc. Natl. Acad. Sci., 112, 3241-3246, doi: 10.1073/pnas.1421533112, 2015.

Kiem, A.S., Johnson, F., Westra, S., van Dijk, A., Evans, J.P., O'Donnell, A., Rouillard, A., Barr, C., Tyler, J., Thyer, M., Jakob, D., Woldemeskel, F., Sivakumar, B., Mehrotra, R.: Nature harzards in Australia: drought, Clim. Change, 139, 37-54, doi:10.1007/s10584-016-1798-7, 2016.

King, A.D., Karoly, D.J., and Henley, B.J.: Australian climate extremes at 1.5°C and 2°C of global warming, Nat. Clim. Change, 7, 412-416, doi:10.1038/nclimate3296, 2017.

Koirala, S., Hirabayashi, Y., Mahendran, R., and Kanae, S,: Global assessment of agreement among streamflow projections using CMIP5 model outputs, Environ. Res. Lett., 9, 064017(11pp), 2014.

Lehner, F., Coats, S., Stocker, T.F., Pendergrass, A.G., Sanderson, B.M., Paible, C.C., and Smerdon, J.E.: Projected drought risk in 1.5°C and 2°C warmer climates, Geophys. Res. Lett., 44, 7419-7428, doi:10.1002/2017GL074117, 2017.

Liu, W.B., Lim, W. H., Sun, F.B., Mitchell, D., Wang, H., Chen, D.L., Bethke, I., Shiogama, H., and Fischer, E.: Global freshwater shortage at low runoff conditions based on HAPPI experiments, Envion. Res. Lett., in review, 2017.

Liu, W.B. and Sun, F.B.: Assessing estimates of evaporative demand in climate models using observed pan evaporation over China, J. Geophys. Res. Atmos., 121, 8329-8349, doi: 10.1002/2016JD025166, 2016.

Liu, W.B. and Sun, F.B.: Projecting and attributing future changes of evaporative demand over China in CMIP5 climate models, J. Hydrometeor., 18, 977-991, doi: 10.1175/JHM-D-16-0204.1, 2017.

Liu, W.B., Wang, L., Chen, D.L., Tu, K., Ruan, C.Q., and Hu, Z.Y.: Large-scale circulation classification and its links to observed precipitation in the eastern and central Tibetan Plateau, Clim. Dyn., 46(11-12), 3481-3497, doi: 10.1007/s00382-015-2782-z, 2016.

Lyon, B.: Seasonal drought in the Greater Horn of Africa and its recent increase during the march-may long rains, J. Clim., 27, 7953-7975, doi:10.1175/JCLI-D-13-00459.1, 2014.

Maraun, D.: Bias correcting climate change simulations – a critical review, Curr. Clim. Change Rep., 2, 211-220, 2016.

Masih, I., Maskey, S., Mussá, F.E.F., and Trambauer, P.: A review of droughts on the African continent: a geospatial and long-term perspective, Hydrol. Earth Syst. Sci., 18, 3635-3649, doi:10.5149/hess-18-3635-2014, 2014.

McKee, T.B., Doesken, N.J. and Kleist, J.: The relationship of drought frequency and duration of time scales, Eighth Conference on Applied Climatology, American Meteorological Society, Jan 17-23, Anaheim CA, PP. 179-186, 1993.

Mishra, A.K. and Singh, V.P.: A review of drought concepts, J. Hydrol., 291, 201-216, doi:10.1016/j.jhydrol.2010.07.012, 2010.

Mitchell, D., James, R., Forster, P.M., Betts, R.A., Shiogama, H., and Allen, M.: Realizing the impacts of a 1.5°C warmer world, Nat. Clim. Change, 6, 735-737, doi:10.10038/nclimate3055, 2016.

Mitchell, D., AchutaRao, K., Allen, M., Bethke, I., Beyerle, U., Ciavarella, A., Forster, P.M., Fuglestvedt, J., Gillett, N., Haustein, K., Ingram, W., Iversen, T., Kharin, V., Klingaman, N., Massey, N., Fischer, E., Schleussner, C.-F., Scinocca, J., Seland, Ø., Shiogama, H., Shuckburgh, E., Sparrow, S., Stone, D., Uhe, P., Wallom, D., Wehner, M., and Zaaboul, R.: Half a degree additional warming, prognosis and projected impacts (HAPPI): background and experimental design, Geosci. Model Dev., 10, 571-583, doi:10.5194/gmd-10-571-2017,2017.

O'Niell, B.C., Tebaldi, C., van Vuuren, D.P., Eyring, C., Friedlingstein, P., Hurtt, G., Knutti, R., Kriegler, E., Lamarque, J.-F., Lowe, J., Meehl, G.A., Moss, R., Riahi, K., and Sanderson, B.M.: The Scenario Model Intercomparison Project (ScenarioMIP) for CMIP6, Geosci. Model Dev., 9, 3461-3482, doi:10.5194/gmd-9-3461-2016, 2016.

Palmer, W.C.: Meteorological drought, U.S. Department of Commerce Weather Bureau Research, Paper 45, 58 pp., 1965.

Peters, G.P.: The "best available science" to inform 1.5°C policy choice, Nat. Clim. Change, 6, 646-649, doi: 10.1038/nclimate3000, 2016.

Qiu, J.: China drought highlights future climate threats, Nature, 465, 142-143, doi:10.1038/465142a, 2010.

Sanderson, B.M., Xu, Y.Y., Tebaldi, C., Wehner, M., O'Neill, B., Jahn, A., Pendergrass, A.G., Lehner, F., Strand, W.G., Lin, L., Knutti, R. and Lamarque, J.F.: Community climate simulations to asses avoided impact in 1.5^{o}C and 2^{o}C futures, Earth Syst. Dyn. Discuss., doi:10.5194/esd-2017-42, 2017.

Schleussner, C., Lissner, T.K., Fischer, E.M., Wohland, J., Perrette, M., Golly, A., Rogelj, J., Childers, K., Schewe, J., Frieler, K., Mengel, M., Hare, W., and Schaeffer, M.: Differential climate impacts for policy-relevant limits to global warming: the case of 1.5^{o}C and 2^{o}C, Earth Syst. Dynam., 7, 327-351, doi: 10.5194/esd-7-327-2016, 2016.

Sheffield, J., Wood, E.F., and Roderick,M.L.: Little change in global drought over the past 60 years, Nature, 491, 435-439, doi:10.1038/nature11575, 2012.

Smirnov, O., Zhang, M.H., Xiao, T.Y., Orbell, J., Lobben, A., and Gordon, J.: The relative importance of climate change and population growth for exposure to future extreme droughts, Clim. Change, 138, 1-2, 41-53, doi: 10.1007/s10584-016-1716-z, 2016.

Sun,F., Roderick, M.L., Lim, W.H., and Farquhar, G.D.: Hydroclimatic projections for the Murray-Darling Basin based on an ensemble derived from Intergovernmental Panel on Climate Change AR4 climate models, Water Resour. Res., 47, W00G02, doi: 10.1029/2010WR009829, 2011.

Taylor, L.E., Stouffer, R.J., and Meehl, G.A.: An Overview of CMIP5 and the Experiment Design, B. Am. Meteorol. Soc., https://doi.org/10.1175/BAMS-D-11-00094.1, 2012.

UNFCCC Conference of the Parties: Adoption of the Paris Agreement, FCCC/CP/2015/10Add.1, 1-32, Paris, 2015.

Van Dijk, A.I.J.M., Beck, H.E., Crosbie, R.S., de Jeu, A.M., Liu, Y.Y., Podger, G.M., Timbal, B., and Viney, N.R.: The Millennium Drought in southeast Australia (2001-2009): Natural and human causes and implications for water resources, ecosystems, economy, and society, Water Resour. Res., 49, 1040-1057, doi:10.1002/wrcr.20123, 2013.

Van Vuuren, D.P., Stehfest, E., Gernaat, D.E.H.J., Doelman, J.C., van den Berg, M., Harmsen, M., de Boer, H.S., Bouwman, L.F., Daioglou, V., Edelenbosch, O.Y., Girod, B., Kram, T., Lassaletta, L., Lucas, P.L., van Meijl, H., Müller, C., van Ruijven, B.J., van der Sluis, S., and Tabeau, A.: Energy, land-use and greenhouse gas emissions trajectories under a green growth paradigm, Global Environ. Chang., 42, 237-250, doi: 10.1016/j.gloenvcha.2016.05.008, 2017.

Wang, A.H., Lettenmaier, and D.P., Sheffield, J.: Soil moisture drought in China, 1950-2006, J. Climate, 24, 3257-3271, doi: 10.1175/2011JCLI3733.1, 2011.

Wang, Z.L., Lin, L., Zhang, X.Y., Zhang, H., Liu, L.K., and Xu, Y.Y.: Scenario dependence of future changes in climate extremes under 1.5^{o}C and 2^{o}C global warming, Sci. Rep., 7:46432, doi:10.1038/srep46432, 2017.

Wells, N., Goddard, S., Hayes, M.J.: A self-calibrating palmer drought severity index, J. Clim., 17, 2335-2351, 2004.

Yevjevich, V., and Ingenieur, J.: An objective approach to definitions and investigations of continental hydrological drought, Water Resource Publ., Fort Collins, 1967.

Zargar, A., Sadiq, R., Naser, B., Khan, F.I.: A review of drought indices, Environ. Rev., 19, 333-349.

Zhang, J., Sun, F.B., Xu, J.J., Chen, Y.N., Sang, Y.-F., and Liu, C.M.: Dependence of trends in and sensitivity of drought over China (1961-2013) on potential evaporation model, Geophys. Res. Lett., 43, 206-213, doi: 10.1002/2015GL067473, 2016.

Zuo, D.D., Hou, W., and Wang, W.X.: Sensitivity analysis of sample number of the drought descriptive model built by Copula function in southwest China, Acta Phys. Sin., 64(10), 100203, doi:10.7498/aps.64.100203,2015

Table 1: Details of CMIP5 climate models applied in this study

Climate models	abbreviation	Horizontal Resolution	Future Scenarios
ACCESS1.0	ACCESS	1.300×1.900 degree	RCP4.5, RCP8.5
BCC_CSM1.1	BCC	2.813×2.791 degree	RCP4.5, RCP8.5
BNU-ESM	BNU	2.810×2.810 degree	RCP4.5, RCP8.5
CanESM23	CANESM	2.813×2.791 degree	RCP4.5, RCP8.5
CNRM-CM5	CNRM	1.406×1.401 degree	RCP4.5, RCP8.5
CSIRO Mk3.6.0	CSIRO	1.875×1.866 degree	RCP4.5, RCP8.5
GFDL CM3	GFDL	2.500×2.000 degree	RCP4.5, RCP8.5
INM-CM4.0	INM	2.000×1.500 degree	RCP4.5, RCP8.5
IPSL-CM5B-LR	IPSL	1.875×3.750 degree	RCP4.5, RCP8.5
MRI-CGCM3	MRI	1.125×1.125 degree	RCP4.5, RCP8.5
MIROC-ESM	MIROC	2.813×2.791 degree	RCP4.5, RCP8.5

Table 2: Definition of regions in this study, after IPCC (2012)

ID	abbreviation	Regional Representation
1	ALA	Alaska/Northwest Canada
2	CGI	East Canada, Greenland, Iceland
3	WNA	West North America
4	CNA	Central North America
5	ENA	East North America
6	CAM	Central America and Mexico
7	AMZ	Amazon
8	NEB	Northeastern Brazil
9	WSA	West Coast South America
10	SSA	Southeastern South America
11	NEU	Northern Europe
12	CEU	Central Europe
13	MED	Southern Europe and Mediterranean
14	SAH	Sahara
15	WAF	West Africa
16	EAF	East Africa
17	SAF	Southern Africa
18	NAS	North Asia
19	WAS	West Asia
20	CAS	Central Asia
21	TIB	Tibetan Plateau
22	EAS	East Asia
23	SAS	South Asia
24	SEA	Southeast Asia
25	NAU	North Australia
26	SAU	South Australia/New Zealand
27	GLOBE	Globe

Figure captions:

Figure 1: Definition of the baseline period, 1.5°C and 2°C warmer worlds based on CMIP5 GCM-simulated changes in global mean temperature (GMT, relative to the pre-industrial levels: 1850-1900). The dark blue and dark yellow shadows indicate the 25th and 75th percentiles of multi-model simulated GMT for RCP 4.5 and RCP 8.5 scenarios, respectively. Both the multi-model ensemble mean and percentiles shown in the figure are smoothed using a moving average approach in a 20-year window

Figure 2: Palmer Drought Severity Index (PDSI)-based drought characteristics definition through the run theory

Figure 3: Changes in multi-model ensemble mean PDSI (i) and model consistency (ii) on a spatial resolution of 0.5° × 0.5°, (a) from the baseline period to 1.5°C warmer world, (b) from the baseline period to 2°C warmer world and (c): (a)-(b). Robustness of projections increases with higher model consistency and vice-versa. The dark-gray boxes show the world regions adopted by IPCC (2012), which are labeled in (a)(i) using the ID numbers defined in Table 2. Legend in (a)(i) applies to (b)(i) and (c)(i); legend in (a)(ii) applies to (b)(ii) and (c)(ii).

Figure 4: Multi-model projected PDSI at the globe (66°N-66°S) and in 27 world regions for the baseline period, 1.5°C and 2°C warmer worlds. The projected uncertainty of multiple climate models is shown through box plots for each region and for each period

Figure 5: Changes in multi-model ensemble mean drought duration (months) (i) and model consistency (ii) on a spatial resolution of 0.5° × 0.5°, (a) from the baseline period to 1.5°C warmer world, (b) from the baseline period to 2°C warmer world and (c) : (a)-(b). The dark-gray boxes show the regions adopted by IPCC (2012), which are labeled in (a)(i) using the ID numbers defined in Table 2. Legend in (a)(i) applies to (b)(i) and (c)(i); legend in (a)(ii) applies to (b)(ii) and (c)(ii).

Figure 6: Multi-model projected drought duration (months) at the globe (66°N-66°S) and in 27 world regions for the baseline period, 1.5°C and 2°C warmer worlds. The projected uncertainty of multiple climate models is shown through box plots for each region and for each period

Figure 7: Changes in multi-model ensemble mean drought intensity (dimensionless) (i) and model consistency (ii) on a spatial resolution of 0.5° × 0.5°, (a) from the baseline period to 1.5°C warmer world, (b) from the baseline period to 2°C warmer world and (c): (a)-(b). The dark-gray boxes show the regions adopted by IPCC (2012), which are labeled in (a)(i) using the ID numbers defined in Table 2. Legend in (a)(i) applies to (b)(i) and (c)(i); legend in (a)(ii) applies to (b)(ii) and (c)(ii).

Figure 8: Multi-model projected drought intensity (dimensionless) at the globe (66°N-66°S) and in 27 world regions for the baseline period, 1.5°C and 2°C warmer worlds. The projected uncertainty of multiple climate models is shown through box plots for each region and for each period

Figure 9: Changes in multi-model ensemble mean drought severity (dimensionless) (i) and model consistency (ii) on a spatial resolution of 0.5° × 0.5°, (a) from the baseline period to 1.5°C warmer world, (b) from the baseline period to 2°C warmer world and (c): (a)-(b). The dark-gray boxes show the regions adopted by IPCC (2012), which are labeled in (a)(i) using the ID numbers defined in Table 2. Legend in (a)(i) applies to (b)(i) and (c)(i); legend in (a)(ii) applies to (b)(ii) and (c)(ii).

Figure 10: Multi-model projected drought severity (dimensionless) at the globe (66°N-66°S) and in 27 world regions for the baseline period, 1.5°C and 2°C warmer worlds. The projected uncertainty of multiple climate models is shown through box plots for each region and for each

period

Figure 11: Multi-model projected frequency (Freq.) and affected total population (Pop., million) of severe drought (PDSI < -3) at the globe and in 27 world regions for the baseline period (black, fixed SSP1 2000 population), 1.5^{o}C (orange, fixed SSP1 2100 population) and 2^{o}C (red, fixed SSP1 2100 population) warmer worlds. The projected uncertainties (standard deviation of multiple-model results) of multiple climate models are shown by error bars (horizontal and vertical)

Figure 12: Multi-model projected frequency (Freq.) and affected urban population (Pop., million) of severe drought (PDSI < -3) at the globe and in 27 regions for the baseline period (black, fixed SSP1 2000 population), 1.5 ^{o}C (orange, fixed SSP1 2100 population) and 2 ^{o}C (red, fixed SSP1 2100 population) warmer worlds. The projected uncertainties (standard deviation of multiple-model results) of multiple climate models are shown by error bars (horizontal and vertical)

Figure 13: Multi-model projected frequency (Freq.) and affected rural population (Pop., million) of severe drought (PDSI < -3) at the globe and in 27 regions for the baseline period (black, fixed SSP1 2000 population), 1.5 ^{o}C (orange, fixed SSP1 2100 population) and 2 ^{o}C (red, fixed SSP1 2100 population) warmer worlds. The projected uncertainties (standard deviation of multiple-model results) of multiple climate models are shown by error bars (horizontal and vertical)

Figure 1: Definition of the baseline period, 1.5°C and 2°C warmer worlds based on CMIP5 GCM-simulated changes in global mean temperature (GMT, relative to the pre-industrial levels: 1850-1900). The dark blue and dark yellow shadows indicate the 25th and 75th percentiles of multi-model simulated GMT for RCP 4.5 and RCP 8.5 scenarios, respectively. Both the multi-model ensemble mean and percentiles shown in the figure are smoothed using a moving average approach in a 20-year window

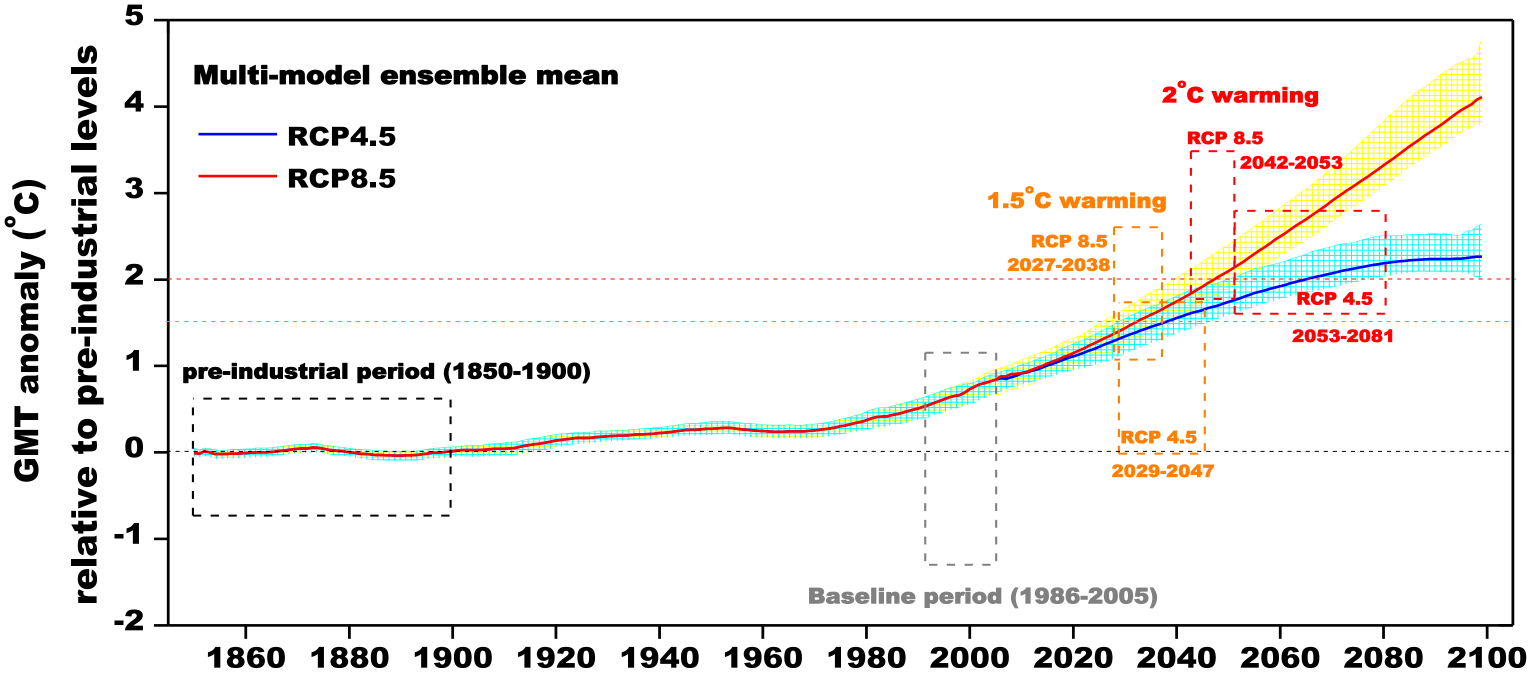

Figure 2: Palmer Drought Severity Index (PDSI)-based drought characteristics definition through the run theory

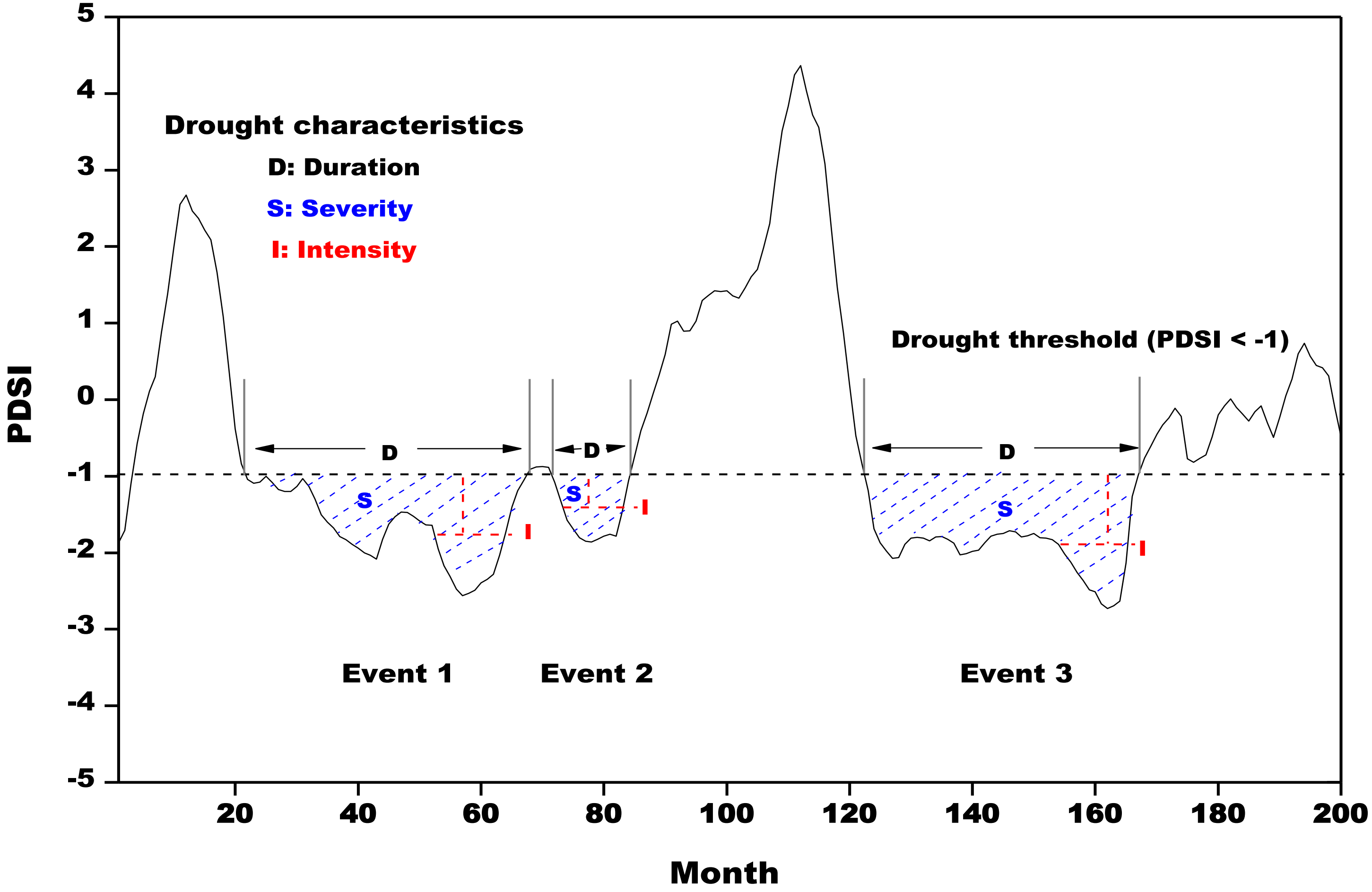

Figure 3: Changes in multi-model ensemble mean PDSI (i) and model consistency (ii) on a spatial resolution of 0.5° × 0.5°, (a) from the baseline period to 1.5°C warmer world, (b) from the baseline period to 2°C warmer world and (c): (a)-(b). Robustness of projections increases with higher model consistency and vice-versa. The dark-gray boxes show the world regions adopted by IPCC (2012), which are labeled in (a)(i) using the ID numbers defined in Table 2. Legend in (a)(i) applies to (b)(i) and (c)(i); legend in (a)(ii) applies to (b)(ii) and (c)(ii).

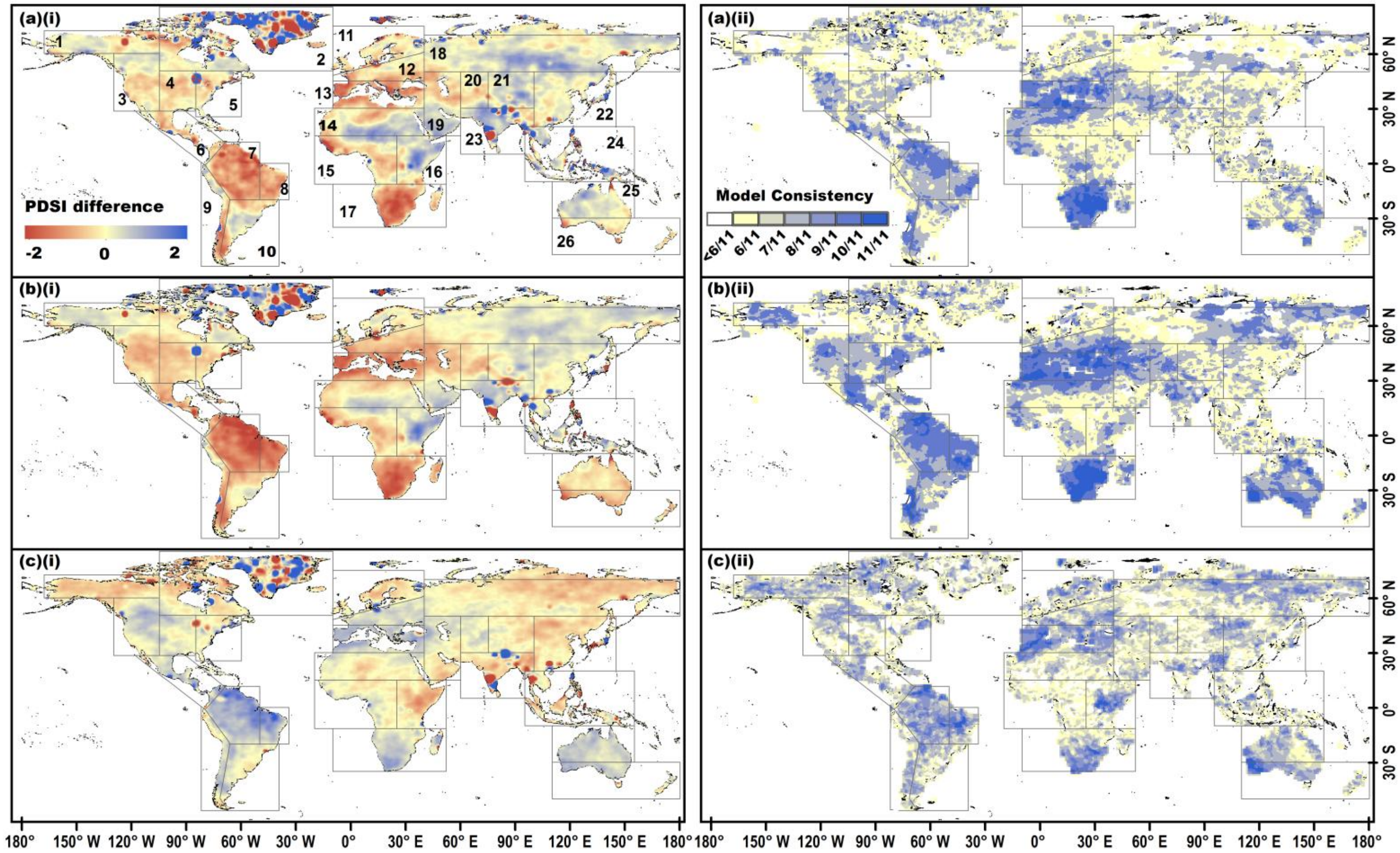

Figure 4: Multi-model projected PDSI at the globe (66°N-66°S) and in 27 world regions for the baseline period, 1.5°C and 2°C warmer worlds. The projected uncertainty of multiple climate models is shown through box plots for each region and for each period

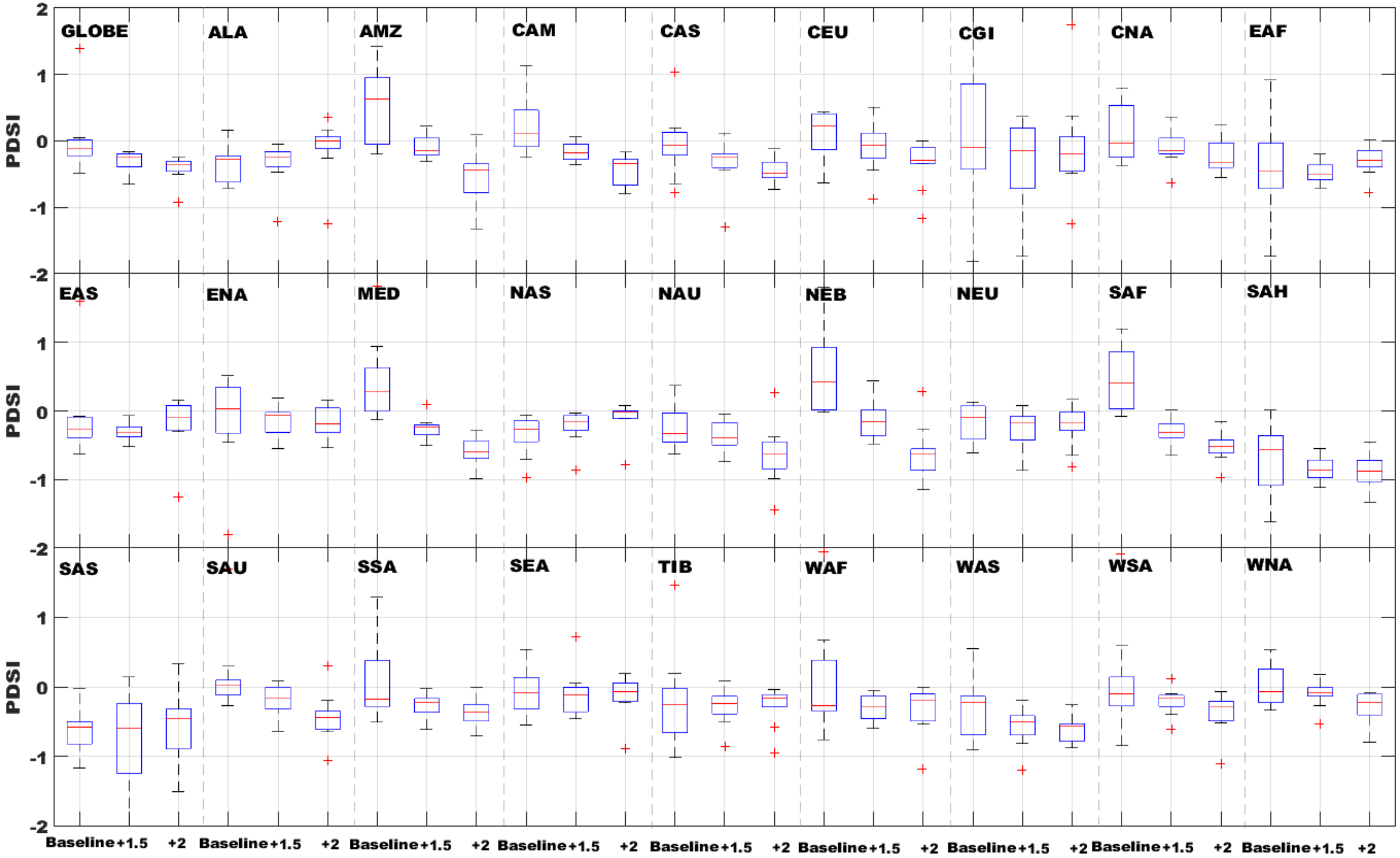

Figure 5: Changes in multi-model ensemble mean drought duration (months) (i) and model consistency (ii) on a spatial resolution of 0.5°× 0.5°, (a) from the baseline period to 1.5°C warmer world, (b) from the baseline period to 2°C warmer world and (c): (a)-(b). The dark-gray boxes show the regions adopted by IPCC (2012), which are labeled in (a)(i) using the ID numbers defined in Table 2. Legend in (a)(i) applies to (b)(i) and (c)(i); legend in (a)(ii) applies to (b)(ii) and (c)(ii).

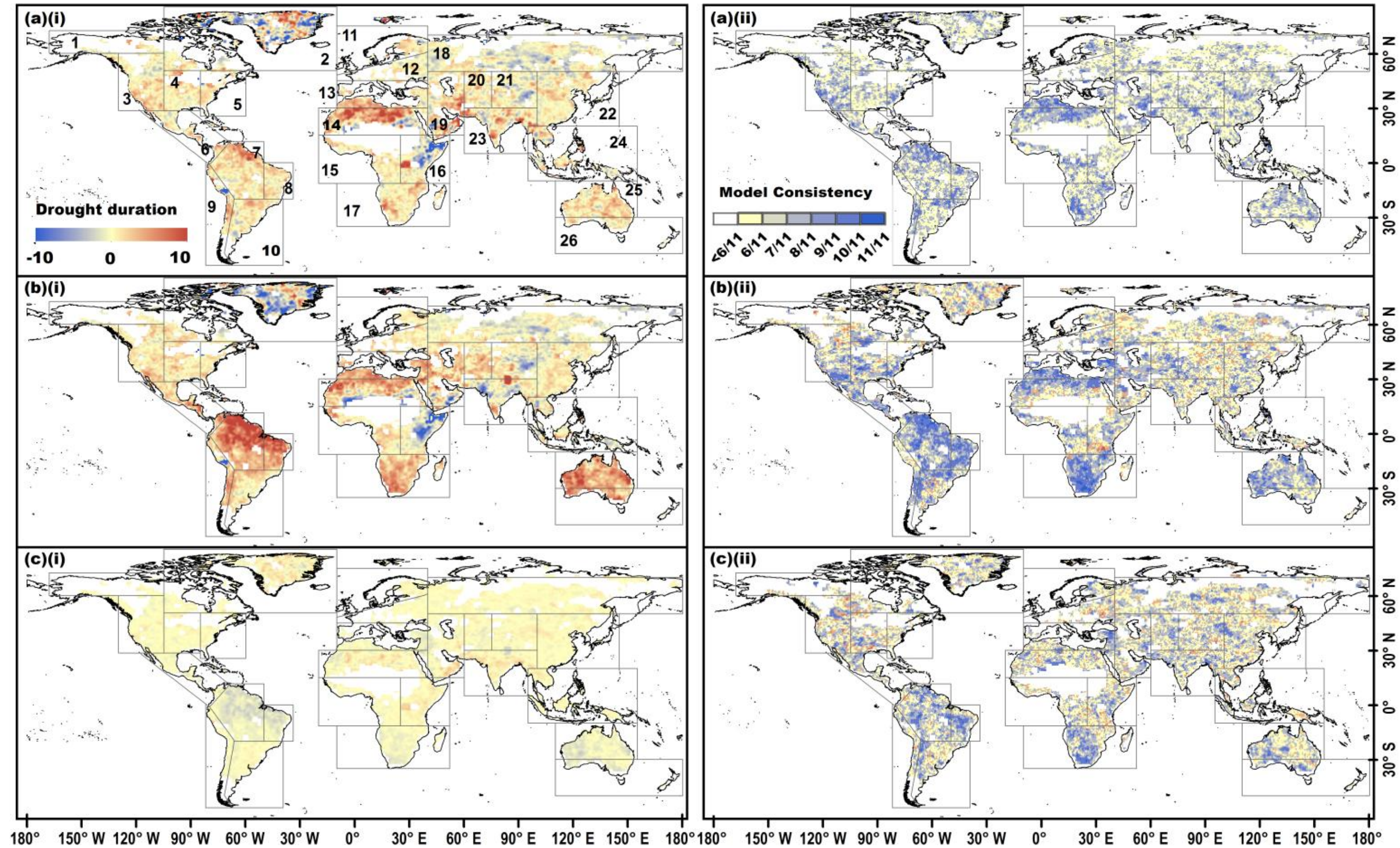

Figure 6: Multi-model projected drought duration (months) at the globe (66°N-66°S) and in 27 regions for the baseline period, 1.5°C and 2°C warmer worlds. The projected uncertainty of multiple climate models is shown through box plots for each region and for each period

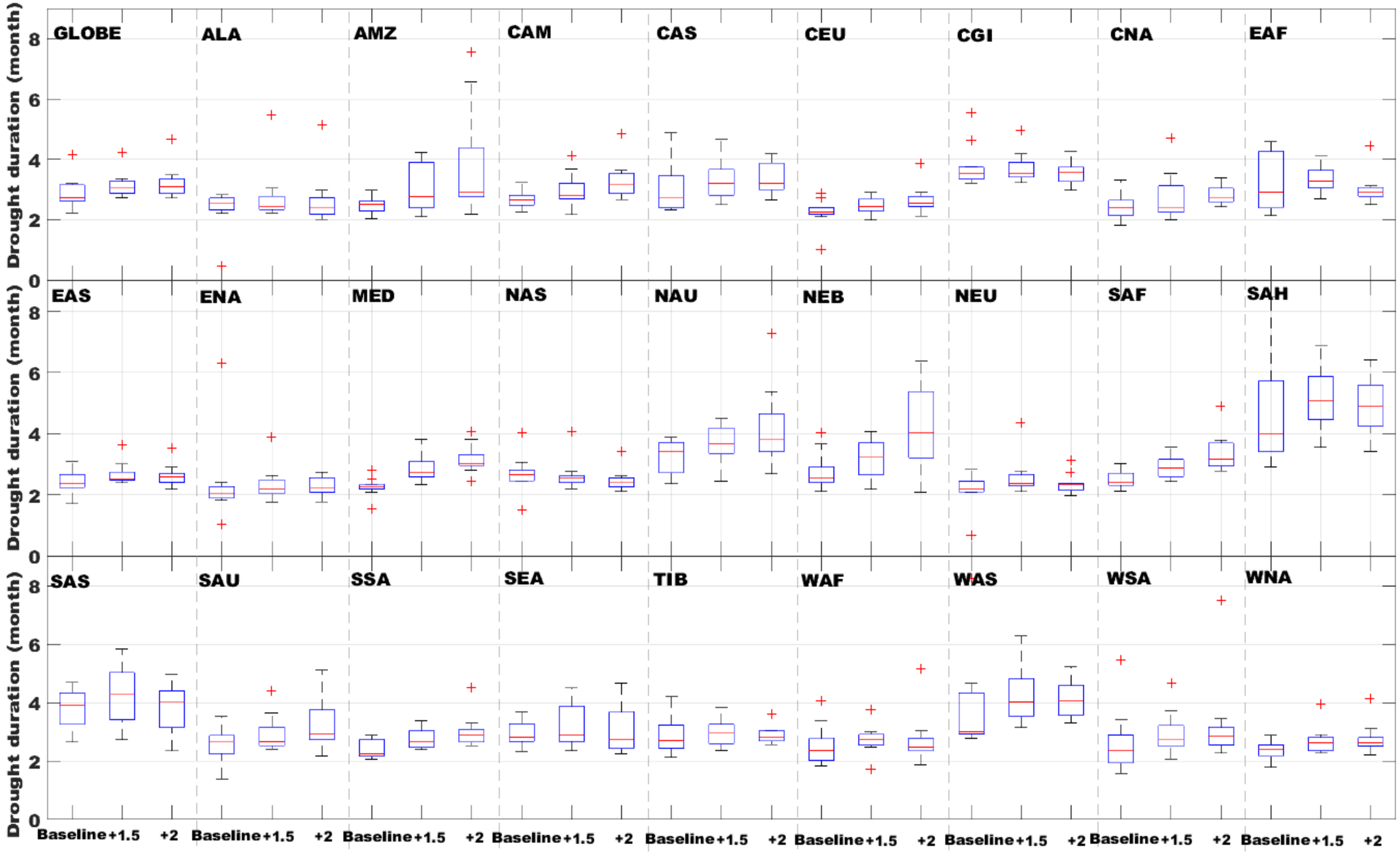

Figure 7: Changes in multi-model ensemble mean drought intensity (dimensionless) (i) and model consistency (ii) on a spatial resolution of 0.5^{o} × 0.5^{o}, (a) from the baseline period to 1.5^{o}C warmer world, (b) from the baseline period to 2^{o}C warmer world and (c): (a)-(b). The dark-gray boxes show the regions adopted by IPCC (2012), which are labeled in (a)(i) using the ID numbers defined in Table 2. Legend in (a)(i) applies to (b)(i) and (c)(i); legend in (a)(ii) applies to (b)(ii) and (c)(ii).

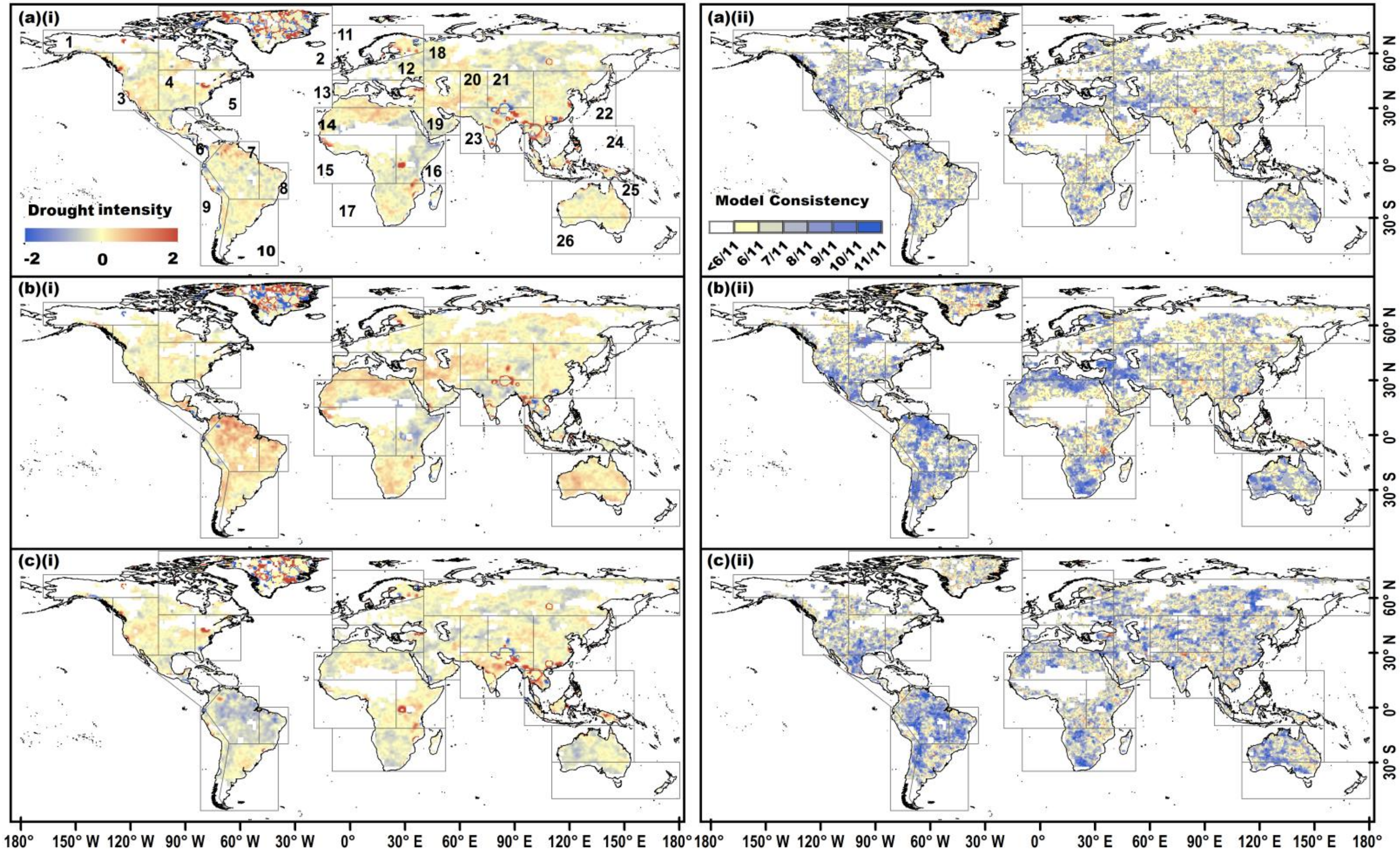

Figure 8: Multi-model projected drought intensity (dimensionless) at the globe (66°N-66°S) and in 27 regions for the baseline period, 1.5°C and 2°C warmer worlds. The projected uncertainty of multiple climate models is shown through box plots for each region and for each period

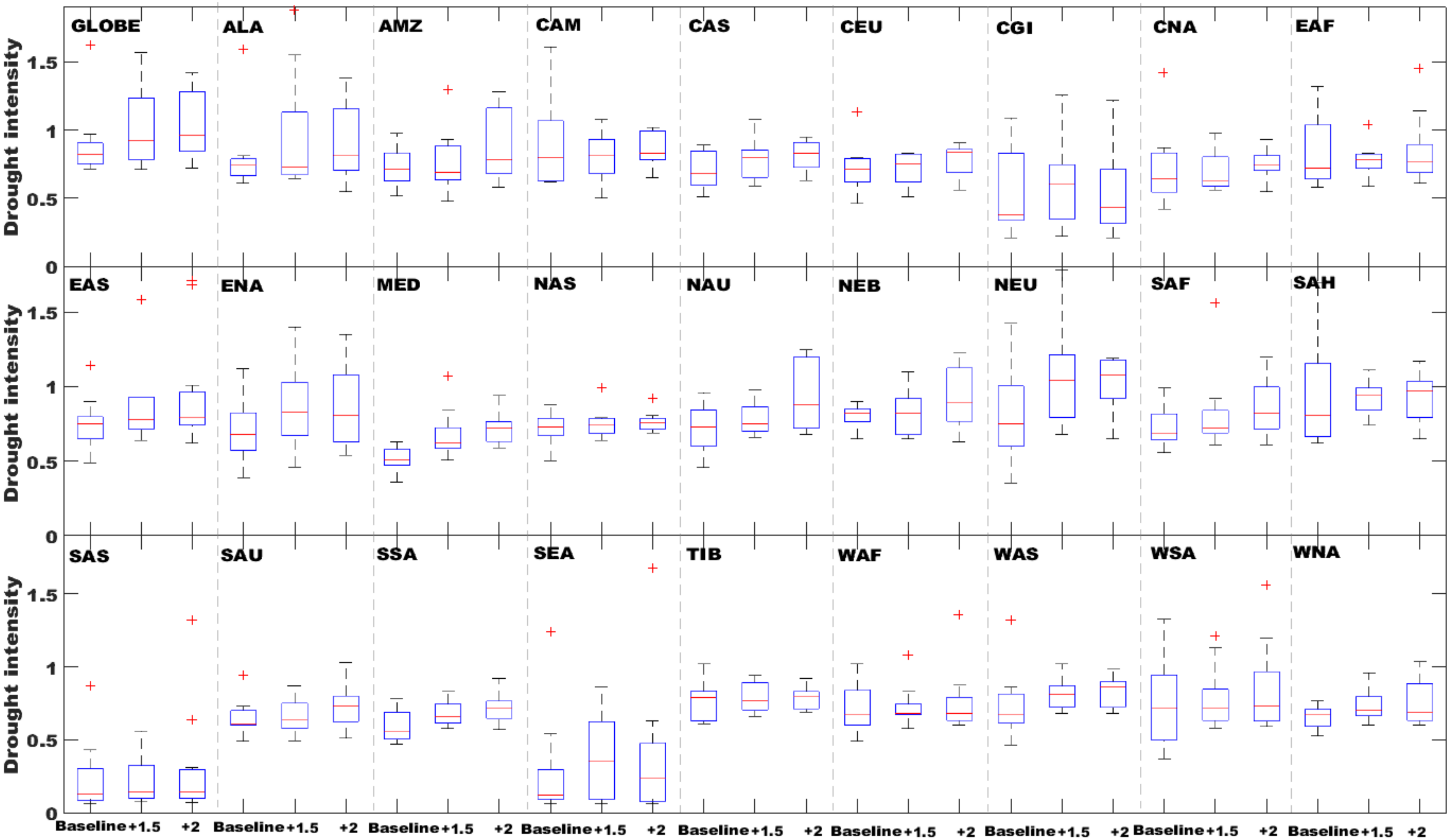

Figure 9: Changes in multi-model ensemble mean drought severity (dimensionless) (i) and model consistency (ii) on a spatial resolution of 0.5^{o} × 0.5^{o}, (a) from the baseline period to 1.5^{o}C warmer world, (b) from the baseline period to 2^{o}C warmer world and (c): (a)-(b). The dark-gray boxes show the regions adopted by IPCC (2012), which are labeled in (a)(i) using the ID numbers defined in Table 2. Legend in (a)(i) applies to (b)(i) and (c)(i); legend in (a)(ii) applies to (b)(ii) and (c)(ii).

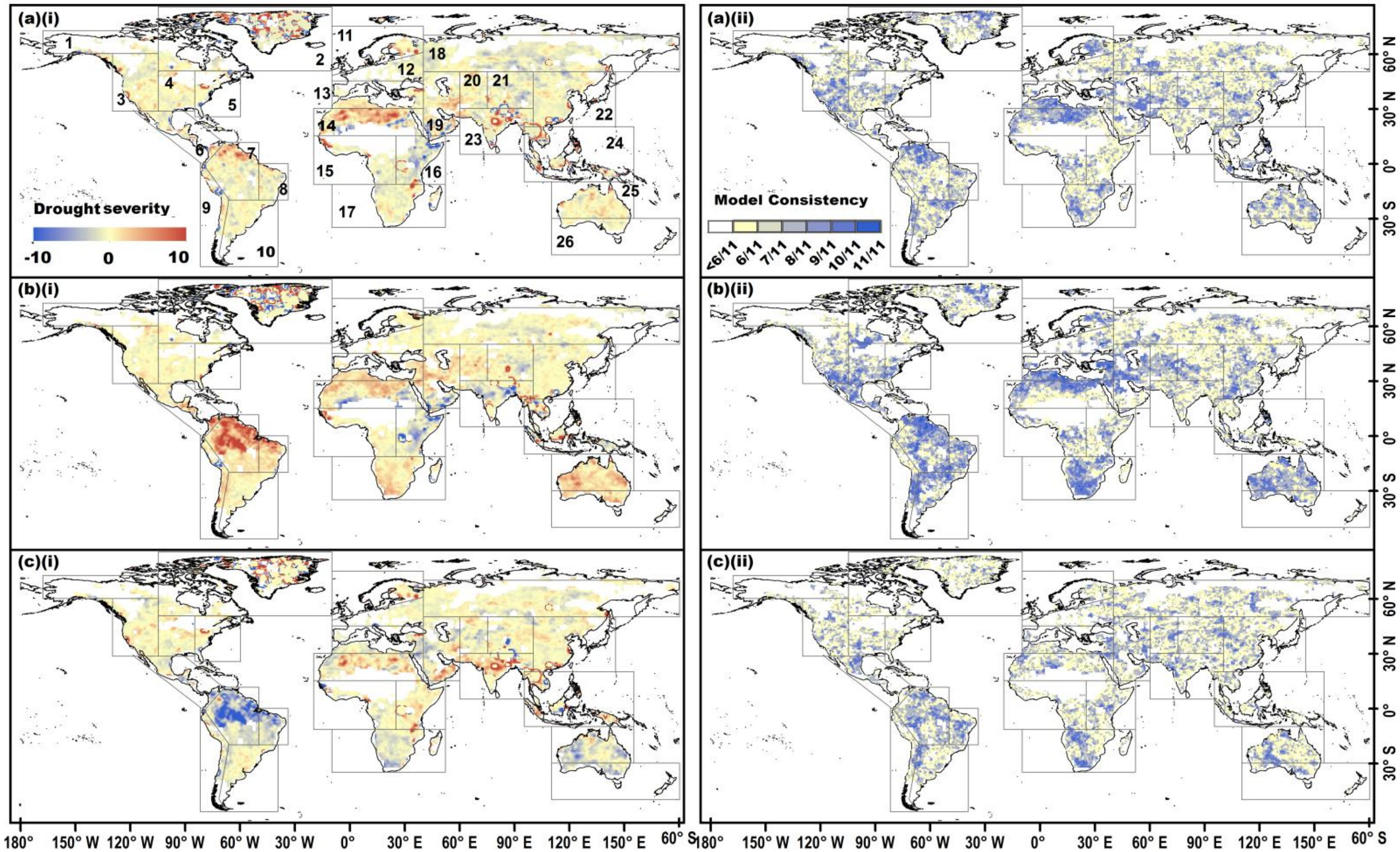

Figure 10: Multi-model projected drought severity (dimensionless) at the globe (66°N-66°S) and in 27 regions for the baseline period, 1.5°C and 2°C warmer worlds. The projected uncertainty of multiple climate models is shown through box plots for each region and for each period

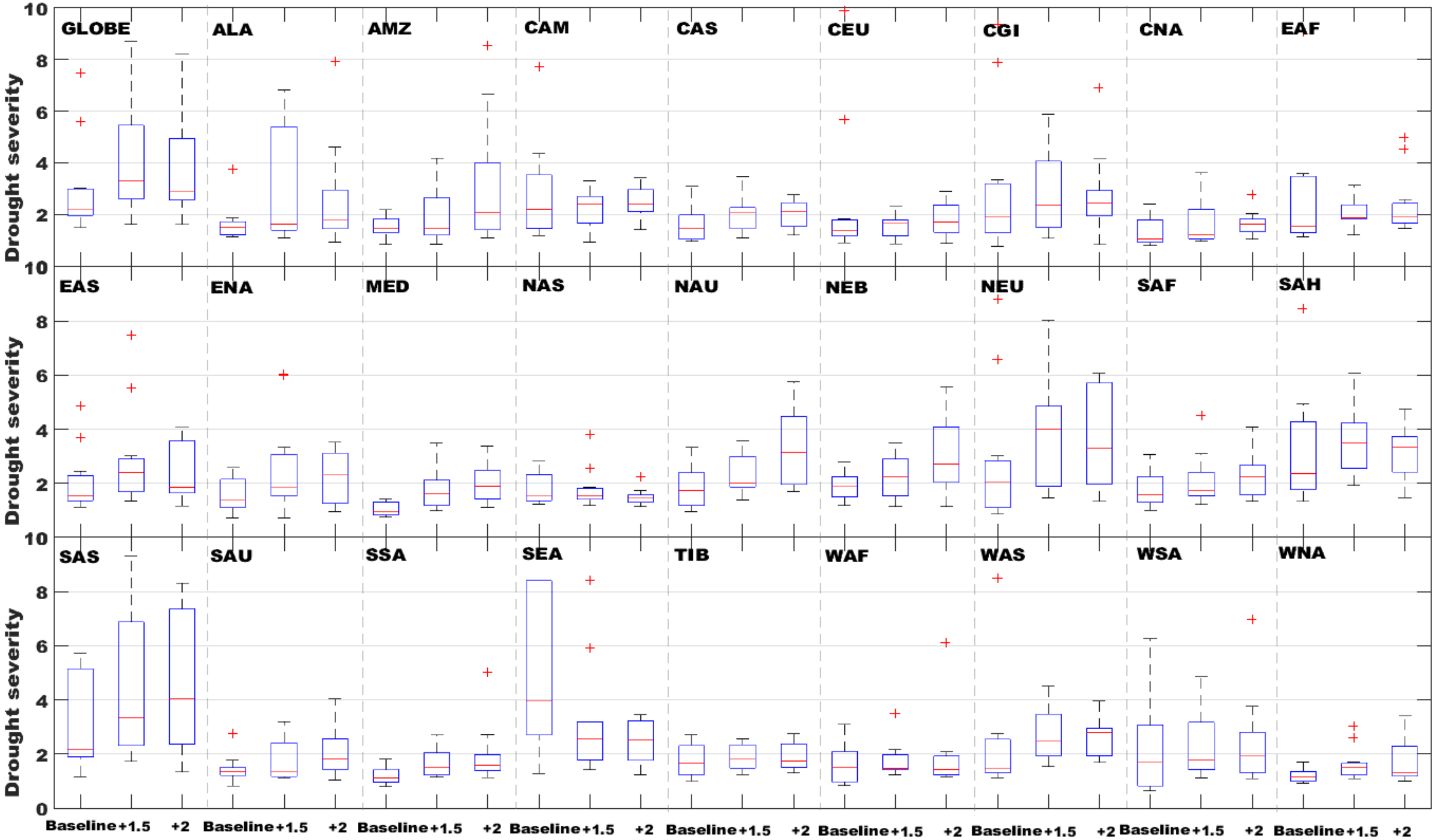

Figure 11: Multi-model projected frequency (Freq.) and affected total population (Pop., million) of severe drought (PDSI < -3) at the globe and in 27 regions for the baseline period (black, fixed SSP1 2000 population), 1.5°C (orange, fixed SSP1 2100 population) and 2°C (red, fixed SSP1 2100 population) warmer worlds. The projected uncertainties (standard deviation of multiple-model results) of multiple climate models are shown by error bars (horizontal and vertical)

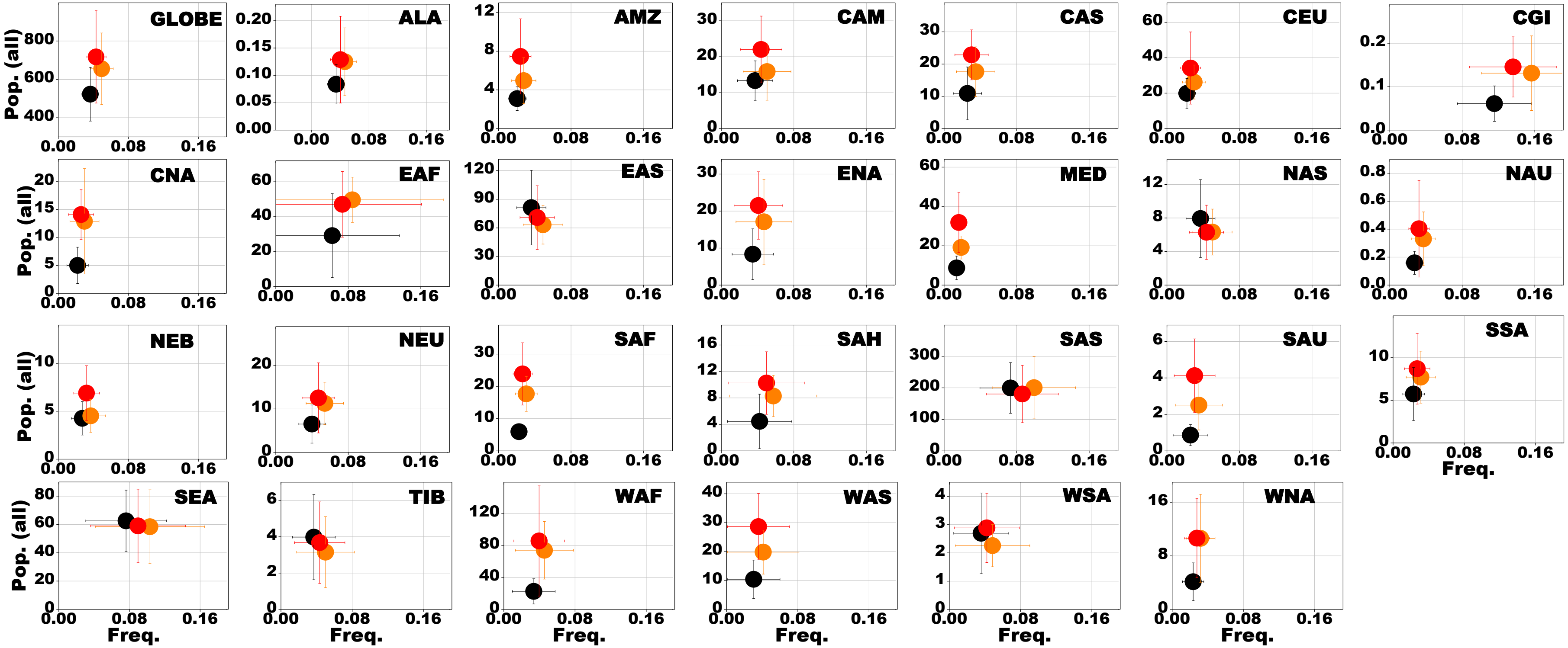

Figure 12: Multi-model projected frequency (Freq.) and affected urban population (Pop., million) of severe drought (PDSI < -3) at the globe and in 27 regions for the baseline period (black, fixed SSP1 2000 population), 1.5°C (orange, fixed SSP1 2100 population) and 2°C (red, fixed SSP1 2100 population) warmer worlds. The projected uncertainties (standard deviation of multiple-model results) of multiple climate models are shown by error bars (horizontal and vertical)

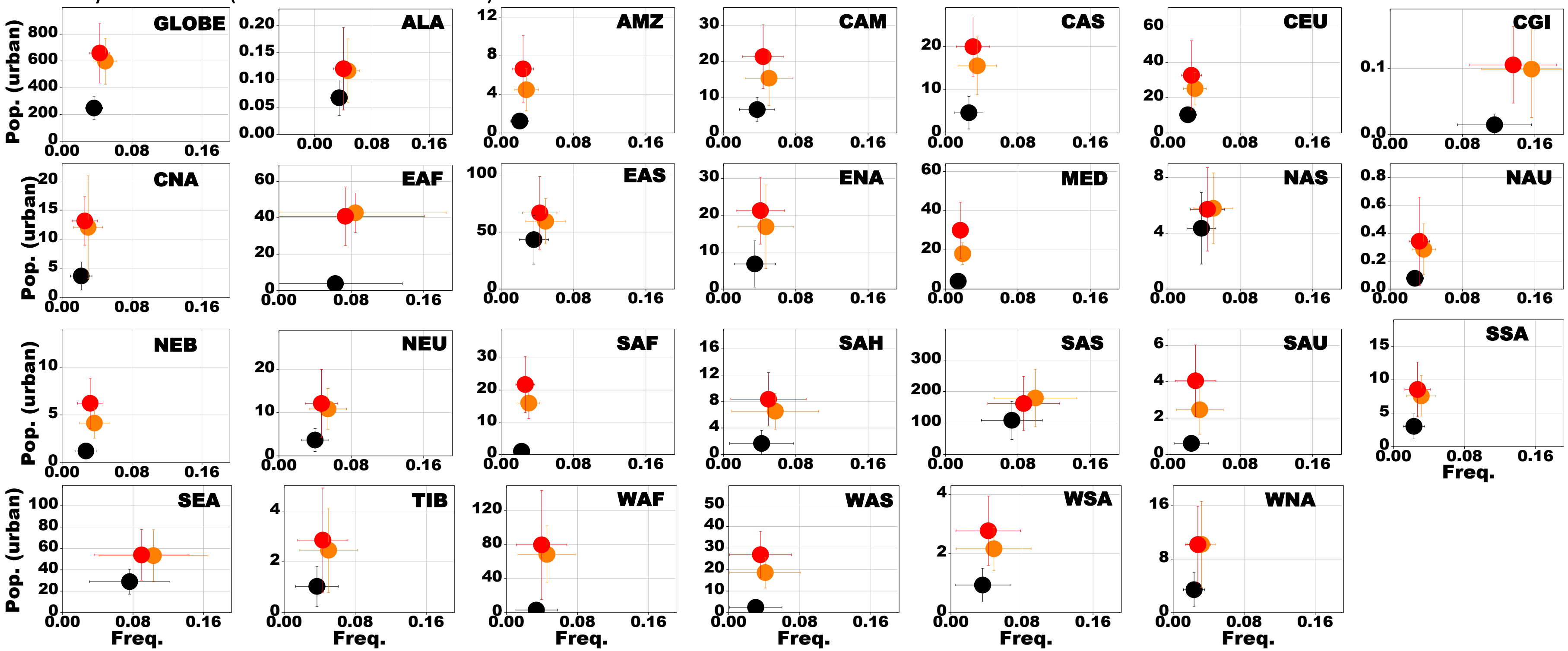

Figure 13: Multi-model projected frequency (Freq.) and affected rural population (Pop., million) of severe drought (PDSI < -3) at the globe and in 27 regions for the baseline period (black, fixed SSP1 2000 population), 1.5°C (orange, fixed SSP1 2100 population) and 2°C (red, fixed SSP1 2100 population) warmer worlds. The projected uncertainties (standard deviation of multiple-model results) of multiple climate models are shown by error bars (horizontal and vertical)